

1 **NO<sub>x</sub> emission estimates during the 2014 Youth Olympic**  
2 **Games in Nanjing**

3

4 **J. Ding<sup>1,2</sup>, R. J. van der A<sup>1</sup>, B. Mijling<sup>1</sup>, P. F. Levelt<sup>1,2</sup>, and N. Hao<sup>3</sup>**

5 [1] Royal Netherlands Meteorological Institute (KNMI), De Bilt, the Netherlands

6 [2] Delft University of Technology, Delft, the Netherlands

7 [3] German Aerospace Center (DLR), Oberpfaffenhofen, Germany

8 Correspondence to: J. Ding (jieying.ding@knmi.nl)

9

10 **Abstract**

11 The Nanjing Government applied temporary environmental regulations to guarantee good air  
12 quality during the Youth Olympic Games (YOG) in 2014. We study the effect of those  
13 regulations by applying the emission estimate algorithm DECSO (Daily Emission estimates  
14 Constrained by Satellite Observations) to measurements of the Ozone Monitoring Instrument  
15 (OMI). We improved DECSO by updating the chemical transport model CHIMERE from  
16 v2006 to v2013 and by adding an Observation minus Forecast (OmF) criterion to filter  
17 outlying satellite retrievals due to high aerosol concentrations. The comparison of model  
18 results with both ground and satellite observations indicates that CHIMERE v2013 is better  
19 performing than CHIMERE v2006. After filtering the satellite observations with high aerosol  
20 loads that were leading to large OmF values, unrealistic jumps in the emission estimates are  
21 removed. Despite the cloudy conditions during the YOG we could still see a decrease of  
22 tropospheric NO<sub>2</sub> column concentrations of about 32% in the OMI observations as compared  
23 to the average NO<sub>2</sub> columns from 2005 to 2012. The results of the improved DECSO  
24 algorithm for NO<sub>x</sub> emissions show a reduction of at least 25% during the YOG period and  
25 afterwards. This indicates that air quality regulations taken by the local government have  
26 effect in reducing NO<sub>x</sub> emissions. The algorithm is also able to detect an emission reduction

1 of 10% during the Chinese Spring Festival. This study demonstrates the capacity of the  
2 DECSO algorithm to capture the change of NO<sub>x</sub> emissions on a monthly scale. We also show  
3 that the observed NO<sub>2</sub> columns and the derived emissions show different patterns that  
4 provide complimentary information. For example, the Nanjing smog episode in December  
5 2013 led to a strong increase in NO<sub>2</sub> concentrations without an increase in NO<sub>x</sub> emissions.  
6 Furthermore, DECSO gives us important information on the non-trivial seasonal relation  
7 between NO<sub>x</sub> emissions and NO<sub>2</sub> concentrations on a local scale.

8

## 9 **1 Introduction**

10 Reducing air pollution is one of the biggest environmental challenges currently in China.  
11 Nearly 75% of urban areas are regularly polluted in a way that was considered unsuitable for  
12 their inhabitants in 2004 (Shao et al., 2006). In mega cities and their immediate vicinities, air  
13 pollutants exceed the Chinese Grade-II standard (80 μg m<sup>-3</sup> for daily NO<sub>2</sub>) on 10-30% in the  
14 days (Chan and Yao, 2008). Air pollution is directly related to the economic growth in China  
15 and its accompanying increase of energy consumption. In the last two decades, air pollutants  
16 persistently increased in China. For instance, satellite measurements showed that NO<sub>2</sub> column  
17 concentrations increased about 50 % from 1996 to 2005 (Irie, 2005; Richter et al., 2005; van  
18 der A et al., 2006). By combining satellite observations with air quality models, Itahashi et al.  
19 (2014) showed that the strong increase of NO<sub>2</sub> columns over East China was caused by a  
20 doubling of NO<sub>x</sub> (NO<sub>x</sub>=NO+NO<sub>2</sub>) emissions during 2000 to 2010. Zhang et al. (2007) found  
21 that NO<sub>x</sub> emissions increased by 70% between 1995 and 2006 and Lamsal et al. (2011) found  
22 that anthropogenic NO<sub>x</sub> emissions increased 18.8% during the period 2006 to 2009.

23 Nanjing, the capital of Jiangsu Province, is a highly urbanized and industrialized city located  
24 in East China, in the northwest part of the Yangtze River Delta (YRD). By 2012, the area of  
25 Nanjing had a population of 8.2 million (Nanjing statistical Bureau, 2013). The YRD is one  
26 of the largest economic and most polluted regions in China. Tu et al. (2007) found that the  
27 largest fraction of air pollution by NO<sub>x</sub> and SO<sub>2</sub> can be attributed to local sources in Nanjing.  
28 Li et al. (2011) concluded that air pollutant concentrations and visibility demanded urgent air  
29 pollution regulations in the YRD region. From 16<sup>th</sup> to 29<sup>th</sup> August 2014, the Youth Olympic  
30 Games (YOG) was held in Nanjing. To guarantee good air quality during the Games, the city

1 government carried out temporary strict environmental regulations with 35 directives from  
2 May to August. Other cities in the YRD cooperated with Nanjing to ensure good air quality  
3 during the Games. The periods with the main regulations are shown in Table 1. In addition,  
4 several technical improvements have been implemented to reduce pollution from heavy  
5 industry and power plants.

6 For previous major international events in China, local authorities have tried to comply with  
7 the air quality standards of the World Health Organization (WHO), which has a limit of 200  
8  $\mu\text{g m}^{-3}$  for hourly  $\text{NO}_2$  concentrations. For each event, the local government imposed  
9 restrictions on heavy industry, construction and traffic. In 2008 the Beijing Municipal  
10 Government implemented a series of air pollution control measures for Beijing and  
11 surrounding cities to guarantee good air quality for the 29<sup>th</sup> Olympic Games. These control  
12 measures significantly reduced the emissions and concentrations of pollutants. Satellite data  
13 show the  $\text{NO}_2$  column concentrations decreased at least 40% compared to previous years  
14 (Mijling et al., 2009; Witte et al., 2009). Both bottom-up and top-down emission estimates  
15 show a decrease of about 40% in  $\text{NO}_x$  emissions (Wang et al., 2009; Wang et al., 2010,  
16 Mijling et al., 2013). During the 2010 World Expo in Shanghai the  $\text{NO}_2$  column was reduced  
17 by 8% from May to August according to an analysis of Hao et al. (2011) of space-based  
18 measurements compared to previous years. In November 2010 emission reduction measures  
19 introduced by the Guangzhou authorities also successfully improved air quality for the Asian  
20 Games. Wu et al. (2013) claimed a  $\text{NO}_x$  emission reduction of 43.5% based on mobile DOAS  
21 measurements. The emission reduction of  $\text{NO}_x$  based on model simulations was estimated to  
22 be about 40% (Liu et al., 2013).

23 However, to study the effectiveness of the air quality measures, it is not enough to look at the  
24 concentration measurements alone, as the reduction of air pollutants can also be affected by  
25 favorable meteorological conditions. Emissions need to be derived to better show the effect  
26 of temporary air quality regulations carried out for the Games. Up-to-date emission data is  
27 difficult to obtain, as most emission inventories are developed by a bottom-up approach  
28 based on statistics on source sector, land-use and sector specific emission factors.

29 The bottom-up approach introduces large uncertainties in the emission inventories. To  
30 improve emission inventories, a top-down approach can be used by estimating emissions  
31 from satellite observations (Streets et al., 2013). For constraining emissions of short-lived  
32 species, Martin et al. (2003) used the ratio of the simulated to the observed column to scale a

1 priori emissions. They used optimal estimation to weigh the a priori emission inventory with  
2 the top-down estimates, resulting in an a posteriori inventory with error estimates. This  
3 method assumes that the relationship between emissions and concentrations is not affected by  
4 transport. Non-linear and non-local relations between emission and concentration can be  
5 indirectly solved by applying the method iteratively (e.g. Zhao and Wang (2009)), although a  
6 posteriori error estimates are lost in this way. Kurokawa et al., (2009) and Stavrou et al.  
7 (2008) used 4DVAR techniques to estimate emissions by applying an adjoint model of the  
8 chemistry transport model to calculate the sensitivities. Another popular data assimilation  
9 method is the Ensemble Kalman Filter (Evensen, 2003), which does not require an adjoint  
10 model and is relatively easy to implement. As an extension of the Kalman filter, it employs a  
11 Monte Carlo approach to represent the uncertainty of the model system with a large  
12 stochastic ensemble. Whenever the filter requires statistics such as mean and covariance,  
13 these are obtained from the sample statistics of the ensemble (Miyazaki et al., 2012).

14 To get fast updates for short lived air pollutants, Mijling and van der A (2012) designed a  
15 Daily Emission estimates Constrained by Satellite Observation (DECSO) algorithm. DECSO  
16 is an inversion method based on an extended Kalman filter. The algorithm only needs one  
17 forward model run of a chemical transport model (CTM) to calculate all local and non-local  
18 emission/concentration relations. It updates emissions by addition instead of scaling, enabling  
19 the detection of unaccounted emission sources.

20 In this study, we use the latest version of DECSO with OMI satellite data to study how the  
21 environmental regulations affect the  $\text{NO}_x$  emissions in Nanjing during the 2014 YOG.  
22 Detecting emission changes for Nanjing is challenging, as it is a smaller city than e.g. Beijing.  
23 In addition, Nanjing is in one of the most populated areas of China close to Shanghai with a  
24 population of about 24 million. Therefore we have introduced a few improvements in the  
25 DECSO algorithm to better resolve small scale emission changes in time and location. The  
26 improvements consist of an updated CTM and better filtering of erroneous satellite  
27 observations. The emission estimates will be based on the satellite observations of OMI,  
28 taking advantage of its high spatial resolution needed to resolve the changes in the Nanjing  
29 area. With this improved algorithm we will compare the  $\text{NO}_x$  emissions during the YOG with  
30  $\text{NO}_x$  emissions of the previous year in the Yangtze Delta River.

31

## 32 **2 Methods**

## 1 2.1 Emission estimates

2 For the emission estimates of NO<sub>x</sub> over China we use the DECSO algorithm (Mijling and van  
3 der A, 2012). It uses a CTM to simulate the NO<sub>2</sub> concentrations and daily satellite  
4 observations of NO<sub>2</sub> column concentrations to constrain NO<sub>x</sub> emissions. The algorithm is  
5 based on an extended Kalman filter to get new emission estimates by optimizing NO<sub>2</sub> column  
6 concentrations of model and satellite observations. The inclusion of sensitivities of NO<sub>2</sub>  
7 column concentrations on the NO<sub>x</sub> emissions in other locations is an essential part of DECSO.  
8 A terrain-following trajectory analysis is used in this calculation to describe the transport of  
9 NO<sub>2</sub> over the model domain for a time interval between two overpasses of the satellite  
10 instrument. This approach results in a fast algorithm suitable for daily estimates of NO<sub>x</sub>  
11 emissions on a 0.25° x 0.25° resolution. A detailed description of DECSO v1 can be found in  
12 Mijling and van der A (2012).

13 The CTM used in DECSO is CHIMERE (Schmidt, 2001; Bessagnet et al., 2004; Menut et al.,  
14 2013). CHIMERE is implemented on a 0.25° x 0.25° spatial grid over East Asia from 18° N  
15 to 50° N and 102° E to 132° E. It contains 8 atmospheric layers up to 500 hPa. The  
16 meteorological input for CHIMERE is the operational meteorological forecast of the  
17 European Centre for Medium-Range Weather Forecasts (ECMWF) with a horizontal  
18 resolution of approximately 25x25 km<sup>2</sup>. The Multi-resolution Emission Inventory for China  
19 (MEIC) (He, 2012) for 2010 gridded to a resolution of 0.25° x 0.25°, is used for the initial  
20 emissions in DECSO. Outside China, where no MEIC emissions are defined, the emission  
21 inventory of INTEX-B (Zhang et al., 2009b) is used. As the emission sector definition used in  
22 MEIC and INTEX-B does not match the 11 activity sectors according to the SNAP (Selected  
23 Nomenclature for Air Pollution) 97, which are internally used in the CHIMERE model, we  
24 estimate the redistribution of the emissions over the sectors (see Table 2).

25 As mentioned by Mijling and van der A (2012), to compare CHIMERE simulations with  
26 satellite observations, we extend the modelled vertical profiles from 500hPa to the tropopause  
27 by adding a climatological partial column, which is from an average of a 2003-2008 run of  
28 the global chemistry transport model TM5. The simulated NO<sub>2</sub> column concentrations on the  
29 model grid are redistributed to the satellite footprints. To enable direct comparison between  
30 simulated and observed tropospheric vertical column, the averaging kernel from the satellite  
31 retrieval is then applied to the modelled vertical profile.

1 In this study, we used an updated version of DECSO, which is referred to as DECSO v3a. In  
2 particular, the calculation speed has been improved in this update. DECSO does not  
3 distinguish between biogenic emissions and the anthropogenic sectorial emissions. Emission  
4 differences are attributed to anthropogenic contribution only, i.e. the biogenic emissions are  
5 assumed to be modeled correctly by the CTM. Emission updates are distributed by ratio over  
6 the sectors (power, industry, transport, domestic) as described by the a priori emission  
7 inventory. If a grid cell is dominated by power plant emissions, however, emission updates  
8 are attributed to the power sector only. The locations of power plants are provided to the  
9 algorithm as additional a priori information. In DECSO v3a, the emission injection height has  
10 been made sector-dependent. Emissions are injected in the lowest three model layers of the  
11 CTM; each sector having its characteristic vertical emission distribution. For example,  
12 transport emissions are released at the surface, while power plant emissions are fully released  
13 in the third model layer corresponding at a typical smokestack height. Trajectory calculations  
14 of the observed species are crucial in the determination of the source-receptor relations. The  
15 DECSO algorithm uses meteorological wind fields (the same as used in the CTM) to  
16 calculate how the content of a tropospheric column is advected over the model domain. Here,  
17 the injection heights is distributed according to the modeled vertical NO<sub>x</sub> distribution. In  
18 DECSO, the forward trajectory calculation is changed to a backward trajectory calculation,  
19 i.e. the source-receptor relations are calculated backward in time, based on the height  
20 distribution of NO<sub>x</sub> modelled at satellite overpass time.

21 In DECSO v3a, tuned synthetic error estimates  $E_{obs}$  estimates are used, derived from the  
22 original satellite observation via :

$$23 \quad E_{obs} = f \cdot E_{sat} + (1 - f) \cdot (0.5 \cdot E_{sat}), \text{ with } f = e^{\left(\frac{-C_{sat}}{2}\right)} \quad (1)$$

24 where  $E_{sat}$  is the original observation error from the retrieval method and  $C_{sat}$  is the retrieved  
25 NO<sub>2</sub> column of the satellite observation. The unit in this formula is 10<sup>15</sup> molecules cm<sup>-2</sup>. The  
26 modified errors give more weight to satellite observations with high values during the  
27 assimilation by reducing their relative error while maintaining the dominating absolute error  
28 for low values (typically around 0.5 10<sup>15</sup> molecules cm<sup>-2</sup>). In this way, DECSO captures  
29 better new emission points or high emission episodes.

30

## 31 **2.2 Satellite observations**

1 In this study, satellite observations from the Dutch-Finnish Ozone Monitoring Instrument  
2 (OMI) on NASA's (National Aeronautics and Space Administration) Aura satellite (Levelt et  
3 al., 2006) are used in DECSO. The satellite was launched on 15 July 2004 into a sun-  
4 synchronous polar orbit at 705 km altitude. OMI is a nadir-viewing spectrometer measuring  
5 the atmosphere-backscattered solar light in the ultraviolet-visible (UV/VIS) range from 270  
6 to 500 nm with a spectral resolution of about 0.5nm. The 114° wide view of OMI results in a  
7 swath width of 2600 km, providing daily global coverage in about 14 orbits. The local  
8 overpass time is around 13:30 local time (LT). The pixel size of OMI is 24x13 km<sup>2</sup> at nadir  
9 and increases to about 150x28 km<sup>2</sup> at the end of the swath.

10 We use the tropospheric NO<sub>2</sub> vertical column concentrations retrieved with the Dutch OMI  
11 NO<sub>2</sub> retrieval (DOMINO) algorithm version 2 (Boersma et al., 2011). The dataset is available  
12 on the Tropospheric Emissions Monitoring Internet Service (TEMIS) portal  
13 (<http://www.temis.nl>). The DOMINO algorithm first obtains NO<sub>2</sub> slant columns from the  
14 OMI reflectance spectra by using Differential Optical Absorption Spectroscopy (DOAS).  
15 After separating the stratospheric and tropospheric contribution to the slant column,  
16 DOMINO converts the tropospheric slant column to a vertical column with the tropospheric  
17 air mass factor (AMF) (Boersma et al., 2007, 2011). DOMINO v2.0 mainly improves the  
18 NO<sub>2</sub> air mass factor by improved radiative transfer, surface albedo, terrain height, clouds and  
19 a priori vertical NO<sub>2</sub> profiles. The bias between DOMINO v2.0 and Multi-Axis Differential  
20 Optical Absorption Spectroscopy (MAX-DOAS) ground observations at 5 locations is only -  
21 10±14% over China and Japan (Irie et al., 2012). The DOMINO algorithm does not explicitly  
22 account for the effect of aerosols on the solar radiation. Rather it is indirectly accounted for  
23 by the higher cloud fraction in aerosol contaminated scenes. However, Lin et al. (2014)  
24 concluded that especially in China the effects of aerosols and surface reflectance anisotropy  
25 have implications for retrievals of NO<sub>2</sub> from OMI and suggested that exclusion of high  
26 aerosol scenes supports better emission estimates at fine spatial and temporal scales.

27 Since 25 June 2007, OMI data has been affected by the so-called row anomaly, which  
28 deteriorates the spectral observations for particular viewing directions of OMI (Boersma et al.,  
29 2011; Kroon et al., 2011). 29 out of the 60 rows are affected by the row anomalies and no  
30 longer used after 1 January 2011. We also filter out the 4 pixels at either side of the swath,  
31 because the size of these pixels is 3 times larger than the model grid cell. After the filtering,  
32 the largest footprint is about 75x21 km<sup>2</sup>. To reduce the influence of cloudy and bright surface

1 scenes on the quality of the retrieval product, we use only observations having a surface  
2 albedo lower than 20% to remove observations over snow and ice (Product Specification  
3 Document of DOMINO v2 on [www.temis.nl](http://www.temis.nl)). The observations with clouds below 800 hPa  
4 are also filtered out as these retrievals are very sensitive to small differences in the NO<sub>2</sub>  
5 profile shape and the retrieved cloud height. Mijling and van der A (2012) filter out the  
6 observations with a cloud fraction higher than 20%. Based on this filtering, there are no  
7 tropospheric NO<sub>2</sub> satellite observations over Nanjing during the YOG due to the cloudy  
8 conditions at the overpass time of the satellite. Thus, to obtain more NO<sub>2</sub> satellite  
9 observations, we use observations with a cloud radiance fraction lower than 70%  
10 (comparable with a cloud fraction of about 30-35%) instead of the cloud fraction lower than  
11 20%. From our analysis of the satellite data we conclude that as a result of this new limit on  
12 the cloud fraction the error on the measurements increases by less than 20% and without  
13 introducing biases. Yet this effect is compensated by the advantage that more data becomes  
14 available. The number of observations over the whole domain increases by about 37 % on  
15 average.

16

### 17 **2.3 Ground-based observations**

18 To validate the model results in Nanjing, we use available independent measurements from  
19 the national in-situ observation network, which are collected and maintained by the China  
20 National Environmental Monitoring Center (CNEMC). The [aqicn.org](http://aqicn.org) team publishes the  
21 hourly Air Quality Index (AQI) of specific air pollutants, such as NO<sub>2</sub>, SO<sub>2</sub>, and particulate  
22 matter (PM<sub>10</sub> and PM<sub>2.5</sub>), on their website based on the measurements from CNEMC. The  
23 AQI is calculated by the conversion table from the Technical Regulation on Ambient Air  
24 Quality Index in China published by the Ministry of Environmental Protection  
25 (<http://kjs.mep.gov.cn/hjbhzbz/bzwb/dqhjbh/jcgfffbz/201203/W020120410332725219541.pdf>  
26 ). We use the same table to convert the AQI back to the surface concentration unit of  $\mu\text{g m}^{-3}$ .  
27 For this study, the NO<sub>2</sub> hourly in-situ measurements of Nanjing for the period of April 2013  
28 to December 2014 are used. The location of these measurements is the Nanjing People's  
29 Government building, which is located in the center of Nanjing. Interpretation of the  
30 validation results is troubled by the absence of peripheral information of the in-situ

1 measurements. For instance, the type of instrument is unknown and the exact location of the  
2 measurement such as the height or the distance to a local traffic road is unclear.

3

### 4 **3 Improvements of DECSO**

#### 5 **3.1 Model improvement**

6 The performance of the CTM is important for the DECSO results. CHIMERE v2006 is an  
7 outdated model version which has been used in DECSO algorithm versions up to v3a. To  
8 improve the emission estimation results, we updated the CTM to CHIMERE v2013 (DECSO  
9 v3b).

10 The new model adds biogenic emissions of six species: isoprene,  $\alpha$ -isoprene,  $\alpha$ -pinene,  $\beta$ -  
11 pinene, limonene, ocimene and NO. These biogenic emissions are calculated by the model  
12 preprocessor using the MEGAN model and land use data (Menut et al., 2013). The added  
13 biogenic emissions can affect the emissions estimated for rural areas as biogenic NO  
14 emissions in rural areas cannot be neglected in summertime. Compared to the old version of  
15 CHIMERE, the new model version includes a more advanced scheme for secondary organic  
16 aerosol chemistry. In addition, the chemical reaction rates are updated and a new transport  
17 scheme is used in the new CHIMERE model. The new CHIMERE model includes the  
18 emission injection height profile for different emission sectors. For CHIMERE v2013 we use  
19 the same input data except for the land use data. We use land use data from the GlobCover  
20 Land Cover (GCLC version 2.3) database, which is updated for the year 2009, while the land  
21 use database included in CHIMERE v2006 is the Global Land Cover Facility (GLFC) giving  
22 the land use of 1994. As China is a fast developing country, the land use may have large  
23 differences in 15 years due to urbanization (see Figure 1). Thus, the updated land use  
24 database will positively affect the model simulations over China.

25 To assess the effect of the new CTM, we run DECSO v3a and DECSO v3b for the period  
26 January 2013 to August 2014. Figure 2 shows the comparison of the average diurnal cycle of  
27 surface NO<sub>2</sub> concentrations from the two CHIMERE models with in-situ observations in  
28 Nanjing averaged for January to August 2014. We select the 0.25°x0.25° model grid cell that

1 contains the in-situ measurement location. According to GCLC database, 70% of the grid cell  
2 is urban area. We see that the surface NO<sub>2</sub> concentration of CHIMERE v2013 during  
3 nighttime is closer to the observations than for CHIMERE v2006. Our earlier model  
4 evaluations of CHIMERE showed that the nocturnal surface NO<sub>2</sub> concentrations simulated by  
5 CHIMERE v2006 are usually too high in urban areas caused by unrealistically low boundary  
6 layer heights and too little vertical diffusion. In CHIMERE v2013, the boundary layer heights  
7 over urban areas are limited by a minimum boundary layer height. As expected, v2013  
8 improves the surface concentration simulation at nighttime, while differences during daytime  
9 are rather small compared to the in-situ observations. We calculate the bias and Root Mean  
10 Square Error (RMSE) between the model results and in-situ observations. The bias of  
11 CHIMERE v2013 is 3.7 μg m<sup>-3</sup>, which is 10 μg m<sup>-3</sup> smaller than for CHIMERE v2006. The  
12 difference of RMSE between the two models is very small, the RMSE of CHIMERE v2013 is  
13 28 μg m<sup>-3</sup> and of CHIMERE v2006 is 31 μg m<sup>-3</sup>. For the satellite overpass time, the bias  
14 improves from 4.4 to 1.8 μg m<sup>-3</sup> while the RMSE remains the same. However, in urban areas  
15 the local sources have transient influences on in-situ observations. Blond et al. (2007)  
16 concluded that urban in-situ observations of NO<sub>2</sub> cannot be used for the validation of a CTM  
17 model with low spatial resolution because the representativeness of the in-situ measurement  
18 for the grid cell is very low. In spite of this, by using the 8-month average of the diurnal cycle  
19 to reduce the transient influences on the in-situ measurements, we see some improvements  
20 for averaged NO<sub>2</sub> concentrations in CHIMERE v2013.

21 In order to get a more comprehensive validation of the model results, we compare the two  
22 CHIMERE models with OMI satellite observations. During the data assimilation of DECSO  
23 the daily “Observation minus Forecasts” (OmF) values have been stored. The OmF is a  
24 common measure for the forecasting capabilities of the model in the data assimilation. We  
25 compare the absolute OmF of both models for the summer (June to August) of 2014 in Figure  
26 3. In the Figure a linear regression is fitted through the data points that shows the absolute  
27 OmF of CHIMERE v2013 is lower than that of CHIMERE v2006 indicating a better  
28 performance of CHIMERE v2013 in summertime. However, the absolute OmF of two  
29 models is similar in wintertime. Since biogenic emissions are negligible in wintertime, this  
30 may point to an effect of the missing biogenic emissions in the older version of CHIMERE.  
31 Based on these comparisons we selected CHIMERE v2013 in DECSO v3b for NO<sub>x</sub> emission  
32 estimates in this study.

1

## 2 **3.2 Quality control of satellite data**

3 Earlier studies showed that the DOMINO v2 retrievals do not account enough for the effect  
4 of high aerosol concentrations on NO<sub>2</sub> columns (see section 2.2) and at the same time we  
5 know that high aerosol concentrations are a significant problem in most megacities in China.  
6 When checking the time series of NO<sub>x</sub> emissions over Nanjing for 2013 by DECSO v3b, we  
7 find some suspicious fluctuations at particular days. At these dates the derived NO<sub>x</sub> emissions  
8 drop to zero in one day and then slowly increase again to the previous emission levels in the  
9 following days. These unrealistic emission updates concurred with extreme OmF values  
10 (lower than -5 or higher than 10 10<sup>15</sup> molecules cm<sup>-2</sup>) with relative small OmF variances,  
11 which are calculated as the quadratic sum of model and observation errors (Figure 4). In the  
12 time period of our study there are 20 days with these extreme OmF values, 6 are positive and  
13 14 are negative. All are having a significant impact on the NO<sub>x</sub> emissions. For most of those  
14 20 days, the in-situ observations of PM10 from CNEMC (see section 2.3) show high aerosol  
15 concentrations, which are above 100 µg m<sup>-3</sup> in Nanjing. We also see a strong haze above  
16 Nanjing for all these 20 days from visual inspection of the MODIS RGB images. In addition,  
17 we noticed that the MODIS images show higher cloud fractions than the fractions retrieved  
18 from OMI observations. The deviating of cloud fraction information from the OMI satellite  
19 retrieval is probably due to the aerosol conditions, which are not taken into account in the  
20 cloud retrieval algorithm (Acarreta et al., 2004; Stammes et al., 2008). High aerosol  
21 concentrations can not only complexly affect the cloud fraction and cloud pressure retrieval  
22 but also directly affect the NO<sub>2</sub> retrieval and results in either over- or under- estimated NO<sub>2</sub>  
23 column concentrations (Lin et al., 2014).

24 Figure 5 shows an example of such an extreme case for East China on 6 May 2013 with high  
25 (positive) OmF values in combination with low observational uncertainties (Eq. 1). In the  
26 image we identify two areas with satellite observations that are at least 10 10<sup>15</sup> molecules cm<sup>-2</sup>  
27 higher than the model forecast. One is over the Hulunbuir sand land at the border of China  
28 and Mongolia, the other one is around the Bohai Bay. We compared the observations with the  
29 MODIS RGB and Aerosol Optical Depth (AOD) images on that day (Figure 6). The MODIS  
30 AOD image shows high aerosol values around the Bohai Bay and over the Hulunbuir sand  
31 land. The RGB image of MODIS shows haze around the Bohai Bay, which indicates that

1 high aerosol concentrations are presented in that area. However, the aerosol information is  
2 not used in the retrieval of the DOMINO NO<sub>2</sub> product leading to NO<sub>2</sub> observations that are  
3 strongly deviating from the model forecast.

4 The effect of high aerosol concentrations on the NO<sub>2</sub> retrieval is non-linear and depends  
5 strongly on both the type of aerosol and its concentration. Also the height of the aerosol layer  
6 and the presence of clouds play a role (Leitão et al., 2010; Lin et al., 2014). It is therefore  
7 difficult to filter out outliers in the observed NO<sub>2</sub> based on aerosol data. In the data  
8 assimilation it is assumed that the OmF distribution is Gaussian and the OmF can be used to  
9 filter outliers from the data. So far, no OmF outlier criterion has been used in DECSO. Our  
10 previous analysis, however, shows the need for the detection of outliers. A filter has to be  
11 implemented with care, to avoid that the algorithm becomes insensitive to new emission  
12 sources such as new power plants. Not losing sensitivity to new emission sources is also the  
13 reason we do not choose a relative filter criterion. We select an OmF filter criterion in the  
14 range of [-5, 10] 10<sup>15</sup> molecules cm<sup>-2</sup> based on our analysis discussed below.

15 The distribution of OmF of all pixels over our domain from January 2013 to September 2014  
16 is Gaussian except for its tails and 97% of the OmF is in the interval of [-5, 10] 10<sup>15</sup>  
17 molecules cm<sup>-2</sup>. However, over highly polluted areas both satellite observations and model  
18 results have larger errors resulting in higher OmF values. In addition, the lifetime of NO<sub>2</sub> is  
19 much longer in winter than in summer. Therefore, the NO<sub>2</sub> column concentration is higher  
20 than in summer, which may lead to large OmF values in winter time. We choose 15 high  
21 polluted cities in China based on AQI and study the distribution of the OmF for the summer  
22 period (April to September, 2013) and the winter period (October, 2013 to March, 2014)  
23 (Figure 7). As expected, the distribution of OmF is wider in winter than in summer. In  
24 summer 70% of the OmF values are in the interval of [-5, 10] 10<sup>15</sup> molecules cm<sup>-2</sup>, while in  
25 winter 50% of the OmF values are within [-5, 10] 10<sup>15</sup> molecules cm<sup>-2</sup>. We select an  
26 asymmetric interval because the assimilation is especially sensitive to very negative outliers  
27 in OmF caused by low observations (having small observational errors associated), as  
28 opposed to very positive outliers caused by high observations, which are associated with  
29 large observational errors. The observations with low error have more weight in the data  
30 assimilation process. To figure out the effect of a large OmF on NO<sub>x</sub> emission estimates, we  
31 compare a free run of CHIMERE v2013 with the MEIC inventory with a run with the  
32 DECSO v3b assimilation. During the summertime, the difference in the seasonal average of

1 the NO<sub>2</sub> column concentration between these two runs is  $4.8 \cdot 10^{15}$  molecules/cm<sup>2</sup> in the  
2 Nanjing area (six grid cells). This column difference is caused by the NO<sub>x</sub> emission  
3 difference of  $9.2 \cdot 10^{15}$  molecules cm<sup>-2</sup> h<sup>-1</sup>. From a simple back-of-the-envelope calculation we  
4 derive that a negative  $5 \cdot 10^{15}$  molecules cm<sup>-2</sup> difference in NO<sub>2</sub> columns requires a  $9.6 \cdot 10^{15}$   
5 molecules cm<sup>-2</sup> h<sup>-1</sup> emission change, which would mean that all NO<sub>x</sub> emissions in Nanjing  
6 would be removed in a single day. This change in emission is comparable to the total  
7 emissions of 2 large-sized coal-fired power plants. This shows that a change in OmF of  $5 \cdot 10^{15}$   
8 molecules cm<sup>-2</sup> is very unrealistic even in the most extreme cases. Therefore, this limit will  
9 be used as a criterion to filter outliers, which are in general caused by wrong NO<sub>2</sub> retrievals.  
10 To avoid the influence of the extreme OmF on emission estimates and still be able to monitor  
11 real emission changes, we filter out negative OmF values lower than  $5 \cdot 10^{15}$  molecules cm<sup>-2</sup>  
12 and positive OmF values more than  $10 \cdot 10^{15}$  molecules cm<sup>-2</sup> to be conservative. After  
13 applying the OmF filter criteria, we filter out 16% of the extreme OmF in the polluted cities  
14 and less than 3% in the whole domain. The large unrealistic jumps in emission disappear  
15 from the time series.

16

#### 17 **4 Emission analysis for the Nanjing Youth Olympic Games**

18 First, we compare NO<sub>2</sub> monthly average concentrations in 2014 with previous years using  
19 in-situ and satellite observations. For the in-situ observations we select the monthly mean at  
20 13:00 LT to be able to compare the results with the satellite observations whose overpass  
21 time is about 13:30 LT (see Figure 8), which is also the average overpass time in Nanjing.  
22 Compared to the year 2013 the in-situ measurements show no significant improvement in the  
23 surface NO<sub>2</sub> concentration at 13:00 LT for the period (May to August, 2014) when the  
24 government took air quality regulations for the YOG. However, we see a high variability in  
25 the monthly averaged data, indicating that the data are strongly affected by highly variable  
26 local sources (e.g. local traffic) and weather. We also calculate the monthly average using all  
27 measurements and we still see a high variability in the time series. Because of the high  
28 variability in the ground data and its low representativity for the whole city of Nanjing, we  
29 discarded this data set in our analysis.”

1 Figure 1 shows the land-use over Jiangsu Province. The rectangle referred to as the Nanjing  
2 area, covers the whole of Nanjing including all industrial areas along Yangtze River.  
3 According to the MEIC sector distribution, the power plants in the selected area are  
4 dominating the NO<sub>x</sub> emissions. To study the effects of the air quality regulations for the YOG  
5 on tropospheric NO<sub>2</sub> column concentrations, we compare the monthly averages of satellite  
6 observations over the Nanjing area for each year from 2005 to 2014 by regridding the  
7 observational data on the model grid over the area.

8 The satellite observations show that on average the NO<sub>2</sub> column concentrations are rather  
9 similar from year to year (Figure 9). Although a small increasing trend from 2005 to 2011 is  
10 visible in the satellite data, it is negligible compared to the SD of the natural variability. It is  
11 clear that the NO<sub>2</sub> columns have a seasonal cycle that is lower in summer than in winter due  
12 to the seasonal change of the NO<sub>2</sub> lifetime (van der A et al., 2006). Note that the small  
13 decrease in columns in February might be caused by the reduced emissions during the Spring  
14 Festival (Zhang et al., 2009b). The monthly averages of NO<sub>2</sub> in-situ observations shown by  
15 Wang et al. (2011) for Beijing, Shanghai and Guangzhou in 2005 were also reduced by  
16 around 10% in February. We see that the NO<sub>2</sub> column during the YOG period (August 2014)  
17 is on average only  $6.6 \times 10^{15}$  molecules cm<sup>-2</sup>, which is the lowest value among the last 10 years  
18 and more than 3 standard deviations from the mean. Possibly due to the effect of the  
19 continuous air quality regulations for the YOG and afterwards, the NO<sub>2</sub> columns of the  
20 following months are also lower than for previous years. The more permanent measures  
21 (traffic-related) resulting from the YOG affect a small fraction of the total emissions. In  
22 November, the local government took similar air quality regulations for the first National  
23 Memorial ceremony held on 13<sup>th</sup> December, 2014. That might explain the lower NO<sub>2</sub>  
24 columns of the last two months of 2014 compared to those of 2013 and compared to the  
25 average of the last 8 years. However, it is still within the range of the standard deviation of  
26 NO<sub>2</sub> columns for the last 8 years. Differences from year to year can also be attributed to the  
27 meteorological conditions (Lin et al., 2011). Particularly in December 2013, NO<sub>2</sub> columns are  
28 very high. This episode is well known as a heavy smog period in Nanjing because stagnant  
29 air in the region accumulated anthropogenic pollution. Compared to the averaged NO<sub>2</sub>  
30 column in August from 2005 to 2012, the NO<sub>2</sub> column of August in 2014 is decreased by 32%  
31 in Nanjing. However, this significant decrease can be caused by the rainy weather during that  
32 month. Thus, NO<sub>x</sub> emission estimates are needed to show if the air quality regulations were  
33 really effective. The emission estimates use not only satellite observations in the location of

1 the YOG but use all observations over China that are transported from and to Nanjing.  
2 Besides transport of air, the meteorological effect on the lifetime of  $\text{NO}_2$  is taken into account.

3 To compare the  $\text{NO}_x$  emissions in Nanjing in 2014, especially during the YOG, with the same  
4 period of the year 2013, we run DECSO v3b with the OmF criterion as described in Section  
5 3.2 from October 2012 to December 2014, where the first three months are used as spin-up  
6 period. Figure 10 shows the monthly  $\text{NO}_x$  emissions in Nanjing for the year 2013 and 2014  
7 estimated by this version of DECSO. For comparison the initial MEIC inventory is also  
8 plotted in the figure. The  $\text{NO}_x$  emissions have a different seasonal cycle compared to the  $\text{NO}_2$   
9 columns of satellite observations in Nanjing. The months with high emissions are June and  
10 July while the highest  $\text{NO}_2$  columns of the satellite observations appear in January and  
11 December. According to the sector distribution in the MEIC inventory, the emissions of  
12 power plants and industrial activities are the main sources in Nanjing. At least 50% of the  
13 total  $\text{NO}_x$  emissions are from power plants and 40% are from the industrial activities. Zhang  
14 et al. (2009) showed that the seasonal cycle of the electricity consumption in Nanjing for the  
15 7 years from 2000 to 2006 peaks in the summertime, because the electricity consumption and  
16 power load are highly correlated with temperature in summer. The value of electricity  
17 consumption in summer is at least two times higher than in winter every year and keeps  
18 increasing during those 7 years. The seasonality of electricity consumption is caused by the  
19 increasing usage of air conditioning in the hot season, while there is no heating system used  
20 in winter time in Nanjing. The opposite cycles of column concentrations (Figure 9) and  
21 emissions (Figure 10) show that the high  $\text{NO}_2$  concentrations in winter in Nanjing are mainly  
22 affected by the long lifetime of  $\text{NO}_x$ , while the seasonal cycle of  $\text{NO}_x$  emissions is reversed as  
23 a result of the increased electricity consumption in summertime. The difference with the  
24 seasonal cycle of MEIC might be attributed to the fact that our results are derived on city-  
25 level, while the seasonal cycle for bottom-up inventories are often derived on a national or  
26 provincial scale (e.g. Zhang et al., 2009b). The monthly average temperatures from June to  
27 September are above 20 degree. The month temperatures in 2014 were not deviating much  
28 from the climatological values.

29 We see a drop in  $\text{NO}_x$  emissions in February for both years calculated with DECSO, which is  
30 also visible in the MEIC inventory of 2010 (Figure 10). This jump is consistent with the  
31 decrease of  $\text{NO}_2$  columns of the satellite observations in February compared to the  
32 neighboring months. Compared to the neighboring months, the  $\text{NO}_x$  emission reduction in

1 February is about 10% in 2013 and 2014. This NO<sub>x</sub> emission decrease was also noticed by  
2 Zhang et al. (2009b) in the INTEX-B inventory and likely to be caused by the reduced  
3 industrial activities during the Spring Festival. Lin and McElroy (2011) also showed that the  
4 Spring Festival causes a reduction of about 10% on NO<sub>x</sub> due to the decrease of thermal power  
5 generation based on the analysis of several satellite observations. Interestingly, we do not see  
6 an increase of NO<sub>x</sub> emissions in the December 2013 smog period. This shows that the smog  
7 is caused by the meteorological conditions rather than increased emissions.

8 Figure 10 shows a large reduction of NO<sub>x</sub> emissions in September, 2014. The total NO<sub>x</sub>  
9 emissions in September in Nanjing are 4.5 Gg N. Compared to the same time of the year  
10 2013, the reduction is about 25%. However, the emission reduction in this case seems to have  
11 a delay of one month. The shaded area in Figure 10 represents the error on the derived  
12 emissions without taking into account the error introduced by the Kalman Filter time lag.  
13 Reductions in emissions at the end of August or the following months can appear with a time  
14 lag in the Kalman filter results (see e.g Brunner et al., 2012). This time lag is not fixed but  
15 depends on the amount, interval, accuracy and distance of the observations and it is therefore  
16 difficult to quantify. In our case, this is partly a consequence of the use of monthly means,  
17 while the regulations became active at the end of August. It is also a consequence of the lack  
18 of satellite observations due to the rainy (and therefore cloudy) weather in the second half of  
19 August 2014 when the YOG took place. For these kind of conditions, DECSO only detects  
20 the full extent of the emission reduction in September. We also see a NO<sub>x</sub> emission reduction  
21 of 10% in August, 2013, compared to the neighboring months. One likely reason for this  
22 reduction is that the Asian Youth Games were held during that time. The local government  
23 also took measures to ensure good air quality for that event but not as strict as for the YOG in  
24 2014. We conclude that the NO<sub>x</sub> emission reduction detected by DECSO for the YOG period  
25 and afterwards was at least 25%, showing that the air quality regulations taken by the local  
26 government were effective.

27

## 28 **5 Discussion and conclusions**

29 In this study the effect of the air quality regulations of the local government during the YOG  
30 in Nanjing in 2014 has been quantified by analyzing observations on the ground and from the

1 satellite. The focus in this study was on the reduced NO<sub>2</sub> concentrations and NO<sub>x</sub> emissions.  
2 We compared NO<sub>2</sub> during the YOG period with previous years using the in-situ and the OMI  
3 satellite observations. The in-situ observations have a large variability, even after averaging  
4 on a monthly basis. This is probably caused by the variability of local sources and it  
5 indicates that these in-situ observations are not representative for the larger area of Nanjing.  
6 The in-situ data shows no significant decrease during the YOG period. Since we have no  
7 error estimates of the in-situ observations and very little information on the instrument and  
8 measurement techniques we discard the results of the in-situ observations in our conclusions.

9 For the view from space we limited ourselves to retrievals of tropospheric NO<sub>2</sub> from OMI,  
10 taking advantage of the high spatial resolution of OMI observations compared to similar  
11 instruments. The monthly OMI satellite observations showed a 32% decrease of the NO<sub>2</sub>  
12 column concentration during the YOG period in Nanjing compared to the average value for  
13 the last 10 years. However, the decrease of NO<sub>2</sub> columns observed by the satellite is not an  
14 objective measure to verify the impact of the air quality regulations taken by the local  
15 government, because changes in NO<sub>2</sub> columns can have more causes such as horizontal  
16 transport of NO<sub>2</sub> or increased wet deposition of the NO<sub>2</sub> reservoir gas NO<sub>3</sub> due to the rainy  
17 weather. Furthermore, due to cloudy conditions, the August average of 2014 is based on few  
18 observations. Therefore, it is important to analyze the emissions to show if the air quality  
19 regulations have really affected the NO<sub>2</sub> concentrations.

20 The results of our improved emission estimate algorithm DECSO show that NO<sub>x</sub> emissions  
21 decreased by at least 25% in September 2014, which shows that the air quality regulations  
22 were effective during the YOG period and that only a small part of the reduced NO<sub>2</sub> column  
23 concentrations were caused by the weather conditions. However, the reduction has one month  
24 delay in our results. This is because satellite observations were scarce in the Nanjing area  
25 during the YOG (16 to 29 August) causing the DECSO algorithm to converge slower to the  
26 new emissions, which is typical for the Kalman filter approach used in DECSO. Although the  
27 strong point of Kalman Filter is its detailed error analysis, this time lag is not incorporated in  
28 its error formalism. In future research we intend to reduce this time lag by using a Smoothing  
29 Kalman Filter technique.

30 We were able to see the emission reduction of NO<sub>x</sub> in the selected 6 grid cells representative  
31 for the Nanjing area. That means that DECSO at least is able to estimate NO<sub>x</sub> emissions on a  
32 spatial resolution of about 50 x 90 km<sup>2</sup>. If we apply the same analysis on single grid cells the

1 results are noisier because the footprint of the OMI covers on average a larger area than a  
2 single grid cell. To achieve emission estimates in a smaller area, either satellite observations  
3 with a higher spatial resolution are required or longer time periods should be considered.

4 The quality of our emission estimates is highly related to the quality of the model and the  
5 satellite observations. We improved the DECSO algorithm by using a new version of the  
6 CTM: CHIMERE v2013 instead of CHIMERE v2006. The comparison of OmF between two  
7 models showed that CHIMERE v2013 has a better performance in summertime. Good quality  
8 of satellite observations is also essential for emission estimates. The DOMINO retrieval  
9 algorithm does not properly account for the effects of high aerosol concentrations, which are  
10 common in China, on the retrieved NO<sub>2</sub> columns. In case of high aerosol concentrations, the  
11 difference of the model simulations and the retrievals is very large, which leads to wrong  
12 updates of NO<sub>x</sub> emission in DECSO. To improve the satellite observations we have set an  
13 OmF criterion to filter out erroneous observations and to avoid unrealistic NO<sub>x</sub> emission  
14 updates. We set the limitation to the range -5 to 10 10<sup>15</sup> molecules cm<sup>-2</sup> for the OmF. With this  
15 filter criterion, the unrealistic updates of NO<sub>x</sub> emissions are mostly prevented. We will  
16 further analyze the impact of high aerosol concentrations on the retrieved NO<sub>2</sub> columns in  
17 future research.

18 Furthermore, we observed an opposite seasonal cycle of NO<sub>x</sub> emissions compared to the NO<sub>2</sub>  
19 columns observed by OMI satellite. The seasonal cycle of NO<sub>x</sub> emissions is not the same for  
20 the whole China domain since the different climate in the North and the South of China leads  
21 to a different seasonality of energy consumption during the year. In Nanjing, as in most parts  
22 of Southern China, people use air conditioning in summer and do not use heating systems in  
23 winter. This leads to a larger electricity production of power plants in summer resulting in  
24 higher NO<sub>x</sub> emissions. Tu et al. (2007) studied the air pollutants in Nanjing and also found  
25 high NO<sub>2</sub> columns in winter but concluded that the high NO<sub>2</sub> columns were caused by high  
26 NO<sub>x</sub> emissions in winter, while our emission estimates show the opposite. Wang et al. (2007)  
27 analyzed the seasonality of NO<sub>x</sub> emissions based on GOME satellite observations for the  
28 regions north and south of Yangtze River, defined as north and south China. Their results of  
29 south China showed the same seasonal cycle of NO<sub>2</sub> columns but a very weak seasonality of  
30 NO<sub>x</sub> emissions and they also concluded that the NO<sub>x</sub> lifetime mainly determines the NO<sub>2</sub>  
31 columns. Ran et al. (2009) explained high NO<sub>x</sub> concentrations in winter are caused by slower  
32 chemical processes and shallow boundary layers contributing to accumulation of NO<sub>x</sub>. The

1 table in Wang et al. (2012) of annual and summer NO<sub>x</sub> emissions from coal-fired power  
2 plants in 2005-2007 for different provinces in China showed that the NO<sub>x</sub> emissions in  
3 Jiangsu Province in summer is higher than mean seasonal emissions.

4 In conclusion, we not only found a reversed seasonal cycle peaking in summertime in the  
5 emission estimates, but also indications for reduced emissions during the Spring Festival, the  
6 Asian Youth Games in 2013 and the YOG 2014. Based on our emission estimates the air  
7 quality regulation during the YOG 2014 and afterwards reduced the NO<sub>x</sub> emissions by at  
8 least 25 percent. This, together with favorable meteorological conditions, was responsible for  
9 a decrease of 32% in NO<sub>2</sub> column concentrations observed from space. For the case of the  
10 YOG, our results can help the local government to identify the impact of their air quality  
11 regulations on reducing NO<sub>x</sub> emissions.

## 12 **Acknowledgement**

13 The research was part of the GlobEmission Project funded and supported by the European  
14 Space Agency. We acknowledge Tsinghua University for providing the MEIC inventory and  
15 the ESA GlobCover 2009 Project for the land use dataset. The MODIS images used in this  
16 study were acquired as part of the NASA's Earth-Sun System Division and archived and  
17 distributed by the MODIS Adaptive Processing System (MODAPS). The OMI is part of the  
18 NASA Earth Observing System (EOS) Aura satellite payload. The OMI project is managed  
19 by the Netherlands Space Office (NSO) and the Royal Netherlands Meteorological Institute  
20 (KNMI).

21

## 22 **Reference**

23 Van der A, R. J., Peters, D. H. M. U., Eskes, H., Boersma, K. F., Van Roozendaal, M., De  
24 Smedt, I. and Kelder, H. M.: Detection of the trend and seasonal variation in tropospheric  
25 NO<sub>2</sub> over China, *J. Geophys. Res.*, 111, D12317, doi:10.1029/2005JD006594, 2006.

26 Acarreta, J. R., De Haan, J. F. and Stammes, P.: Cloud pressure retrieval using the O<sub>2</sub>-O<sub>2</sub>  
27 absorption band at 477 nm, *J. Geophys. Res.*, 109(D5), D05204, doi:10.1029/2003JD003915,  
28 2004.

- 1 Bessagnet, B., Hodzic, A., Vautard, R., Beekmann, M., Cheinet, S., Honoré, C., Liousse, C.  
2 and Rouil, L.: Aerosol modeling with CHIMERE—preliminary evaluation at the continental  
3 scale, *Atmos. Environ.*, 38(18), 2803–2817, doi:10.1016/j.atmosenv.2004.02.034, 2004.
- 4 Blond, N., Boersma, K. F., Eskes, H. J., van der A, R. J., Van Roozendael, M., De Smedt, I.,  
5 Bergametti, G. and Vautard, R.: Intercomparison of SCIAMACHY nitrogen dioxide  
6 observations, in situ measurements and air quality modeling results over Western Europe, *J.*  
7 *Geophys. Res.*, 112(2), 1–20, doi:10.1029/2006JD007277, 2007.
- 8 Boersma, K. F., Eskes, H. J., Dirksen, R. J., van der A, R. J., Veefkind, J. P., Stammes, P.,  
9 Huijnen, V., Kleipool, Q. L., Sneep, M., Claas, J., Leitão, J., Richter, a., Zhou, Y. and  
10 Brunner, D.: An improved tropospheric NO<sub>2</sub> column retrieval algorithm for the Ozone  
11 Monitoring Instrument, *Atmos. Meas. Tech.*, 4(9), 1905–1928, doi:10.5194/amt-4-1905-2011,  
12 2011.
- 13 Boersma, K. F., Eskes, H. J., Veefkind, J. P., Brinksma, E. J., Sneep, M., Oord, G. H. J. Van  
14 Den, Levelt, P. F., Stammes, P. and Gleason, J. F.: Near-real time retrieval of tropospheric  
15 NO<sub>2</sub> from OMI, *Atmos. Chem. Phys.*, 7(8), 2103–2118, 2007.
- 16 Brunner, D., Henne, S., Keller, C. A., Reimann, S., Vollmer, M. K., O’Doherty, S. and  
17 Maione, M.: An extended Kalman-filter for regional scale inverse emission estimation,  
18 *Atmos. Chem. Phys.*, 12(7), 3455–3478, doi:10.5194/acp-12-3455-2012, 2012.
- 19 Chan, C. and Yao, X.: Air pollution in mega cities in China, *Atmos. Environ.*, 42(1), 1–42,  
20 doi:10.1016/j.atmosenv.2007.09.003, 2008.
- 21 Evensen, G.: The Ensemble Kalman Filter: theoretical formulation and practical  
22 implementation, *Ocean Dyn.*, 53(4), 343–367, doi:10.1007/s10236-003-0036-9, 2003.
- 23 Hao, N., Valks, P., Loyola, D., Cheng, Y. F. and Zimmer, W.: Space-based measurements of  
24 air quality during the World Expo 2010 in Shanghai, *Environ. Res. Lett.*, 6(4), 044004,  
25 doi:10.1088/1748-9326/6/4/044004, 2011.
- 26 He, K.: Multi-resolution Emission Inventory for China (MEIC): model framework and 1990-  
27 2010 anthropogenic emissions, in International Global Atmospheric Chemistry Conference,  
28 17-21 September, Beijing, China. [online] Available from:  
29 <http://adsabs.harvard.edu/abs/2012AGUFM.A32B..05H> (Accessed 4 February 2015), 2012.
- 30 Irie, H.: Evaluation of long-term tropospheric NO<sub>2</sub> data obtained by GOME over East Asia in  
31 1996–2002, *Geophys. Res. Lett.*, 32(11), L11810, doi:10.1029/2005GL022770, 2005.
- 32 Irie, H., Boersma, K. F., Kanaya, Y., Takashima, H., Pan, X. and Wang, Z. F.: Quantitative  
33 bias estimates for tropospheric NO<sub>2</sub> columns retrieved from SCIAMACHY, OMI, and  
34 GOME-2 using a common standard for East Asia, *Atmos. Meas. Tech.*, 5(10), 2403–2411,  
35 doi:10.5194/amt-5-2403-2012, 2012.
- 36 Itahashi, S., Uno, I., Irie, H., Kurokawa, J.-I. and Ohara, T.: Regional modeling of  
37 tropospheric NO<sub>2</sub> vertical column density over East Asia during the period 2000–2010:  
38 comparison with multisatellite observations, *Atmos. Chem. Phys.*, 14(7), 3623–3635,  
39 doi:10.5194/acp-14-3623-2014, 2014.

- 1 Kroon, M., de Haan, J. F., Veeffkind, J. P., Froidevaux, L., Wang, R., Kivi, R. and  
2 Hakkarainen, J. J.: Validation of operational ozone profiles from the Ozone Monitoring  
3 Instrument, *J. Geophys. Res.*, 116(D18), D18305, doi:10.1029/2010JD015100, 2011.
- 4 Kurokawa, J., Yumimoto, K., Uno, I. and Ohara, T.: Adjoint inverse modeling of NO<sub>x</sub>  
5 emissions over eastern China using satellite observations of NO<sub>2</sub> vertical column densities,  
6 *Atmos. Environ.*, 43(11), 1878–1887, doi:10.1016/j.atmosenv.2008.12.030, 2009.
- 7 Lamsal, L. N., Martin, R. V., Padmanabhan, A., van Donkelaar, A., Zhang, Q., Sioris, C. E.,  
8 Chance, K., Kurosu, T. P. and Newchurch, M. J.: Application of satellite observations for  
9 timely updates to global anthropogenic NO<sub>x</sub> emission inventories, *Geophys. Res. Lett.*, 38(5),  
10 L05810, doi:10.1029/2010GL046476, 2011.
- 11 Leitão, J., Richter, A., Vrekoussis, M., Kokhanovsky, A., Zhang, Q. J., Beekmann, M. and  
12 Burrows, J. P.: On the improvement of NO<sub>2</sub> satellite retrievals – aerosol impact on the  
13 airmass factors, *Atmos. Meas. Tech.*, 3(2), 475–493, doi:10.5194/amt-3-475-2010, 2010.
- 14 Levelt, P. F., van den Oord, G. H. J., Dobber, M. R., Malkki, A., Stammes, P., Lundell, J. O.  
15 V. and Saari, H.: The ozone monitoring instrument, *IEEE Trans. Geosci. Remote Sens.*, 44(5),  
16 1093–1101, doi:10.1109/TGRS.2006.872333, 2006.
- 17 Li, L., Chen, C. H., Fu, J. S., Huang, C., Street, D. G., Huang, H. Y., Zhang, G. F., Wang, Y.  
18 J., Jiang, C. J., Wang, H. L., Chen, Y. R. and Fu, J. M.: Air quality and emissions in the  
19 Yangtze River Delta, China, *Atmos. Chem. Phys.*, 11(4), 1621–1639, doi:10.5194/acp-11-  
20 1621-2011, 2011.
- 21 Lin, J.-T., Martin, R. V., Boersma, K. F., Sneep, M., Stammes, P., Spurr, R., Wang, P., Van  
22 Roozendaal, M., Clémer, K. and Irie, H.: Retrieving tropospheric nitrogen dioxide from the  
23 Ozone Monitoring Instrument: effects of aerosols, surface reflectance anisotropy, and vertical  
24 profile of nitrogen dioxide, *Atmos. Chem. Phys.*, 14(3), 1441–1461, doi:10.5194/acp-14-  
25 1441-2014, 2014.
- 26 Lin, J.-T. and McElroy, M. B.: Detection from space of a reduction in anthropogenic  
27 emissions of nitrogen oxides during the Chinese economic downturn, *Atmos. Chem. Phys.*,  
28 11(15), 8171–8188, doi:10.5194/acp-11-8171-2011, 2011.
- 29 Lin, W., Xu, X., Ge, B. and Liu, X.: Gaseous pollutants in Beijing urban area during the  
30 heating period 2007–2008: variability, sources, meteorological, and chemical impacts, *Atmos.*  
31 *Chem. Phys.*, 11(15), 8157–8170, doi:10.5194/acp-11-8157-2011, 2011.
- 32 Liu, H., Wang, X., Zhang, J., He, K., Wu, Y. and Xu, J.: Emission controls and changes in air  
33 quality in Guangzhou during the Asian Games, *Atmos. Environ.*, 76, 81–93,  
34 doi:10.1016/j.atmosenv.2012.08.004, 2013.
- 35 Martin, R. V., Jacob, D. J., Kurosu, T. P., Chance, K., Palmer, P. I. and Evans, M. J.: Global  
36 inventory of nitrogen oxide emissions constrained by space-based observations of NO<sub>2</sub>  
37 columns, *J. Geophys. Res.*, 108(D17), 4537, doi:10.1029/2003JD003453, 2003.
- 38 Menut, L., Bessagnet, B., Khvorostyanov, D., Beekmann, M., Blond, N., Colette, A., Coll, I.,  
39 Curci, G., Foret, G., Hodzic, A., Mailler, S., Meleux, F., Monge, J.-L., Pison, I., Siour, G.,

- 1 Turquety, S., Valari, M., Vautard, R. and Vivanco, M. G.: CHIMERE 2013: a model for  
2 regional atmospheric composition modelling, *Geosci. Model Dev.*, 6(4), 981–1028,  
3 doi:10.5194/gmd-6-981-2013, 2013.
- 4 Mijling, B. and van der A, R. J.: Using daily satellite observations to estimate emissions of  
5 short-lived air pollutants on a mesoscopic scale, *J. Geophys. Res. Atmos.*, 117, D17302,  
6 doi:10.1029/2012JD017817, 2012.
- 7 Mijling, B., van der A, R. J., Boersma, K. F., Van Roozendaal, M., De Smedt, I. and Kelder,  
8 H. M.: Reductions of NO<sub>2</sub> detected from space during the 2008 Beijing Olympic Games,  
9 *Geophys. Res. Lett.*, 36(13), L13801, doi:10.1029/2009GL038943, 2009.
- 10 Miyazaki, K., Eskes, H. J., Sudo, K., Takigawa, M., Weele, M. van and Boersma, K. F.:  
11 Simultaneous assimilation of satellite NO<sub>2</sub>, O<sub>3</sub>, CO, and HNO<sub>3</sub> data for the analysis of  
12 tropospheric chemical composition and emissions, *Atmos. Chem. Phys.*, 12(20), 9545–9579,  
13 doi:10.5194/acp-12-9545-2012, 2012.
- 14 Ran, L., Zhao, C., Geng, F., Tie, X., Tang, X., Peng, L., Zhou, G., Yu, Q., Xu, J. and  
15 Guenther, A.: Ozone photochemical production in urban Shanghai, China: Analysis based on  
16 ground level observations, *J. Geophys. Res.*, 114(D15), D15301, doi:10.1029/2008JD010752,  
17 2009.
- 18 Richter, A., Burrows, J. P., Nüss, H., Granier, C. and Niemeier, U.: Increase in tropospheric  
19 nitrogen dioxide over China observed from space., *Nature*, 437(7055), 129–32,  
20 doi:10.1038/nature04092, 2005.
- 21 Schmidt, H.: A comparison of simulated and observed ozone mixing ratios for the summer of  
22 1998 in Western Europe, *Atmos. Environ.*, 35(36), 6277–6297, doi:10.1016/S1352-  
23 2310(01)00451-4, 2001.
- 24 Shao, M., Tang, X., Zhang, Y. and Li, W.: City clusters in China: air and surface water  
25 pollution, *Front. Ecol. Environ.*, 4(7), 353–361, doi:10.1890/1540-  
26 9295(2006)004[0353:CCICAA]2.0.CO;2, 2006.
- 27 Stammes, P., Sneep, M., de Haan, J. F., Veefkind, J. P., Wang, P. and Levelt, P. F.: Effective  
28 cloud fractions from the Ozone Monitoring Instrument: Theoretical framework and validation,  
29 *J. Geophys. Res.*, 113(D16), D16S38, doi:10.1029/2007JD008820, 2008.
- 30 Stavrakou, T., Müller, J.-F., Boersma, K. F., De Smedt, I. and van der A, R. J.: Assessing the  
31 distribution and growth rates of NO<sub>x</sub> emission sources by inverting a 10-year record of NO<sub>2</sub>  
32 satellite columns, *Geophys. Res. Lett.*, 35(10), doi:10.1029/2008GL033521, 2008.
- 33 Streets, D. G., Canty, T., Carmichael, G. R., de Foy, B., Dickerson, R. R., Duncan, B. N.,  
34 Edwards, D. P., Haynes, J. A., Henze, D. K., Houyoux, M. R., Jacob, D. J., Krotkov, N. A.,  
35 Lamsal, L. N., Liu, Y., Lu, Z., Martin, R. V., Pfister, G. G., Pinder, R. W., Salawitch, R. J.  
36 and Wecht, K. J.: Emissions estimation from satellite retrievals: A review of current  
37 capability, *Atmos. Environ.*, 77, 1011–1042, doi:10.1016/j.atmosenv.2013.05.051, 2013.

- 1 Tu, J., Xia, Z.-G., Wang, H. and Li, W.: Temporal variations in surface ozone and its  
2 precursors and meteorological effects at an urban site in China, *Atmos. Res.*, 85(3-4), 310–  
3 337, doi:10.1016/j.atmosres.2007.02.003, 2007.
- 4 Wang, S. W., Zhang, Q., Streets, D. G., He, K. B., Martin, R. V., Lamsal, L. N., Chen, D.,  
5 Lei, Y. and Lu, Z.: Growth in NO<sub>x</sub> emissions from power plants in China: bottom-up  
6 estimates and satellite observations, *Atmos. Chem. Phys.*, 12(10), 4429–4447,  
7 doi:10.5194/acp-12-4429-2012, 2012.
- 8 Wang, S., Xing, J., Chatani, S., Hao, J., Klimont, Z., Cofala, J. and Amann, M.: Verification  
9 of anthropogenic emissions of China by satellite and ground observations, *Atmos. Environ.*,  
10 45(35), 6347–6358, doi:10.1016/j.atmosenv.2011.08.054, 2011.
- 11 Wang, S., Zhao, M., Xing, J., Wu, Y., Zhou, Y., Lei, Y., He, K., Fu, L. and Hao, J.:  
12 Quantifying the air pollutants emission reduction during the 2008 olympic games in Beijing,  
13 *Environ. Sci. Technol.*, 44(7), 2490–2496, 2010.
- 14 Wang, Y., Hao, J., McElroy, M. B., Munger, J. W., Ma, H., Chen, D. and Nielsen, C. P.:  
15 Ozone air quality during the 2008 Beijing Olympics: effectiveness of emission restrictions,  
16 *Atmos. Chem. Phys.*, 9(14), 5237–5251, doi:10.5194/acp-9-5237-2009, 2009.
- 17 Wang, Y., McElroy, M. B., Martin, R. V., Streets, D. G., Zhang, Q. and Fu, T. M.: Seasonal  
18 variability of NO<sub>x</sub> emissions over east China constrained by satellite observations:  
19 Implications for combustion and microbial sources, *J. Geophys. Res. Atmos.*, 112(x), 1–19,  
20 doi:10.1029/2006JD007538, 2007.
- 21 Witte, J. C., Schoeberl, M. R., Douglass, A. R., Gleason, J. F., Krotkov, N. A., Gille, J. C.,  
22 Pickering, K. E. and Livesey, N.: Satellite observations of changes in air quality during the  
23 2008 Beijing Olympics and Paralympics, *Geophys. Res. Lett.*, 36(17), L17803,  
24 doi:10.1029/2009GL039236, 2009.
- 25 Wu, F. C., Xie, P. H., Li, A., Chan, K. L., Hartl, A., Wang, Y., Si, F. Q., Zeng, Y., Qin, M.,  
26 Xu, J., Liu, J. G., Liu, W. Q. and Wenig, M.: Observations of SO<sub>2</sub> by mobile DOAS in the  
27 Guangzhou eastern area during the Asian Games 2010, *Atmos. Meas. Tech.*, 6(9), 2277–2292,  
28 doi:10.5194/amt-6-2277-2013, 2013.
- 29 Zhang, H., Sun, Z., Zhen, Y., Zhang, X. and Yu, B.: Impact of Temperature Change on  
30 Urban Electric Power Load in Nanjing, *Transactions Atmos. Sci.*, 32(4), 536–542, 2009a.
- 31 Zhang, Q., Streets, D. G., Carmichael, G. R., He, K., Huo, H., Kannari, a., Klimont, Z., Park,  
32 I., Reddy, S., Fu, J. S., Chen, D., Duan, L., Lei, Y., Wang, L. and Yao, Z.: Asian emissions in  
33 2006 for the NASA INTEX-B mission, *Atmos. Chem. Phys. Discuss.*, 9, 4081–4139,  
34 doi:10.5194/acpd-9-4081-2009, 2009b.
- 35 Zhang, Q., Streets, D. G., He, K., Wang, Y., Richter, A., Burrows, J. P., Uno, I., Jang, C. J.,  
36 Chen, D., Yao, Z. and Lei, Y.: NO<sub>x</sub> emission trends for China, 1995–2004: The view from  
37 the ground and the view from space, *J. Geophys. Res.*, 112, D22306,  
38 doi:10.1029/2007JD008684, 2007.

1 Zhao, C. and Wang, Y.: Assimilated inversion of NO<sub>x</sub> emissions over east Asia using OMI  
2 NO<sub>2</sub> column measurements, *Geophys. Res. Lett.*, 36(6), L06805,  
3 doi:10.1029/2008GL037123, 2009.

4

- 1 Table 1. Air quality regulations taken by the Nanjing authorities in the year of YOG2014.  
 2 The period is the start time of different regulations. The underline regulations are still  
 3 effective after the YOG.

Period	Regulations
<b>1<sup>st</sup> May - 30<sup>th</sup> June</b>	The local government started to shut down the coal-burning factories.
<b>1<sup>st</sup> July - 15<sup>th</sup> July</b>	All coal-burning factories have been shut down.
<b>16<sup>th</sup> July - 31<sup>st</sup> July</b>	The work on one third of construction sites was stopped. The parking fees in downtown increased sevenfold.
<b>1<sup>st</sup> August – 15<sup>th</sup> August</b>	The work on 2000 construction sites was stopped. Heavy-industry factories reduced manufacturing by 20 percent. <u>Vehicles with high emissions were banned from the city.</u> Open space barbecue restaurants were closed. <u>900 electric buses and 500 taxis have been put into operation.</u>
<b>16<sup>th</sup> August-31<sup>st</sup> August</b>	The work at all construction sites was put on hold.

4

5

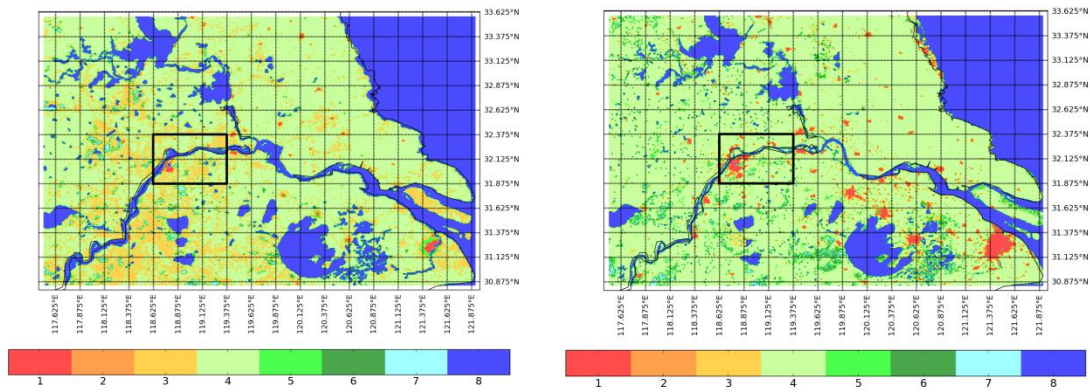
1 Table 2. Estimated redistribution of MEIC sectors over SNAP 97 sectors

MEIC sectors SNAP 97 sectors	Power	Industry	Transport	Residential	Agriculture
Combustion in energy and transformation industries	1	-	-	-	-
Non-industrial combustion plants	-	-	-	1	-
Combustion in manufacturing industry	-	0.3	-	-	-
Production process	-	0.3	-	-	-
Extraction and distribution of fossil fuels and geothermal energy	-	0.4	-	-	-
Solvent and other product use	-	-	-	-	-
Road transport	-	-	1	-	-
Other mobile sources and machinery	-	-	-	-	-
Waste treatment and disposal	-	-	-	-	-
Agriculture	-	-	-	-	1
Other source and sinks	-	-	-	-	-

2

3

4

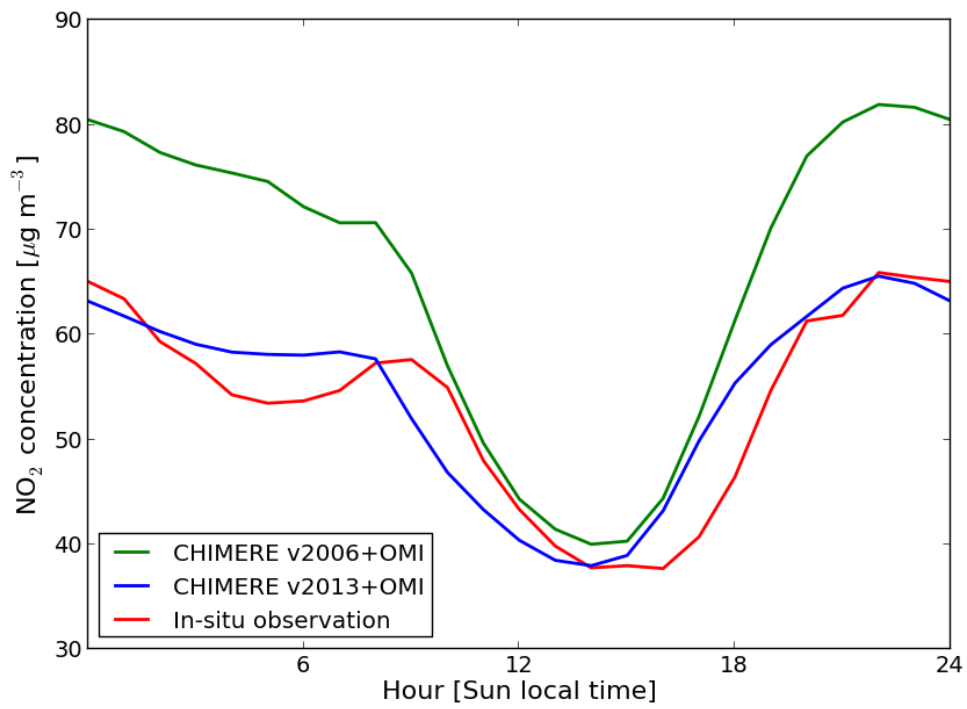


1

2

3 Figure 1. Land use over the Jiangsu Province from Global Land Cover Facility (1994) (left)  
 4 and the GlobCover Land Cover (2009) (right) and as used in CHIMERE v2006 and  
 5 CHIMERE v2013. The 8 categories are: 1. Urban, 2. Barren land, 3. Grassland, 4.  
 6 Agricultural land, 5. Shrubs, 6. Needleleaf forest, 7. Broadleaf forest, 8. Water. The solid  
 7 rectangle (about 50 x 90 km<sup>2</sup>) indicates the 6 grid cells that cover the Nanjing area.

8

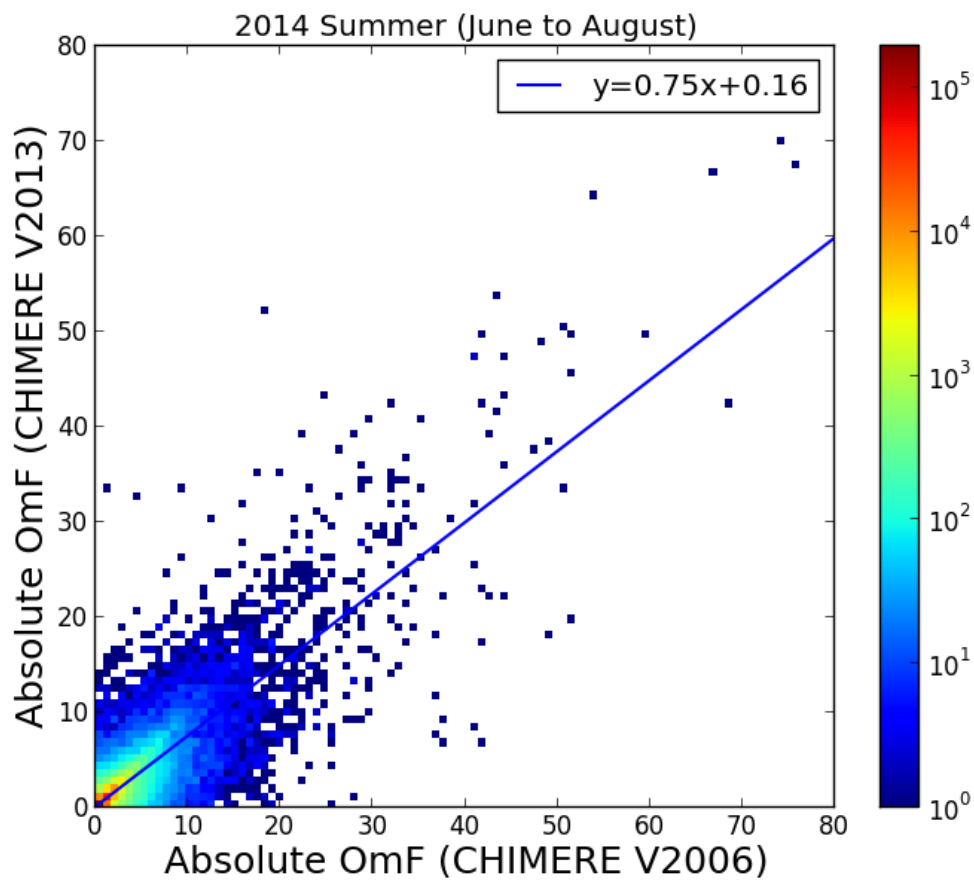


1

2

3 Figure 2. The diurnal cycle in Nanjing from January to August 2014 according in-situ  
 4 observations, OMI-assimilated CHIMERE v2013 and CHIMERE v2006.

5

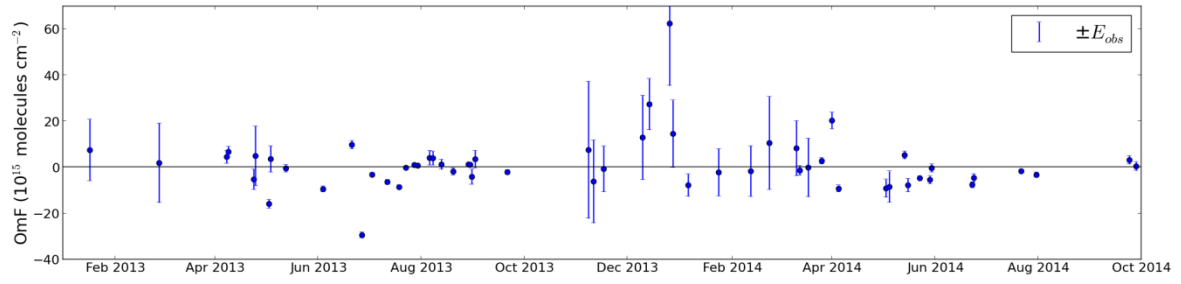


1

2

3 Figure 3. The comparison of the absolute OmF ( $10^{15}$  molecules/cm<sup>2</sup>) of CHIMERE v2006  
 4 and CHIMERE v2013 for the whole East Asian domain from June to August . The colorbar  
 5 represents the frequency of satellite observations for that specific value of OmF.

6

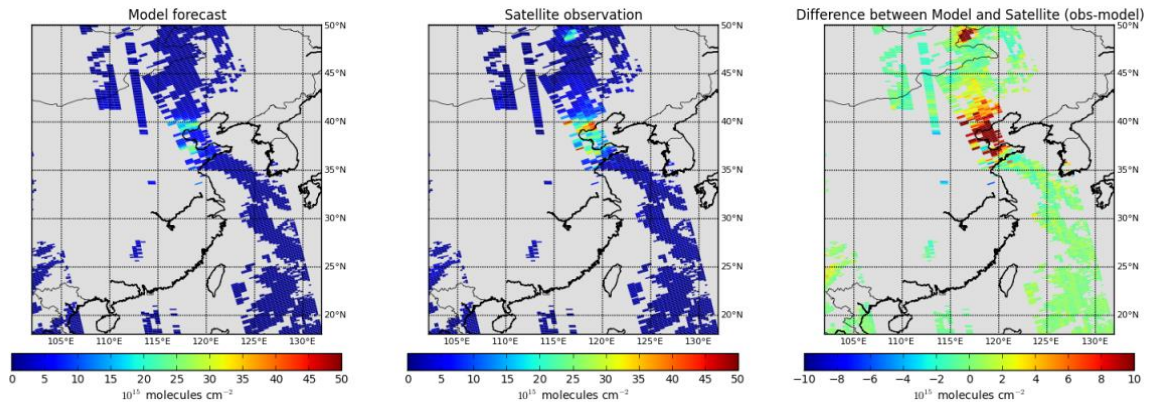


1

2

3 Figure 4. The time series of the OmF from January 2013 to September 2014 for the single  
4 grid cell over the center of Nanjing. The error bar is the root mean square error of  
5 observations ( $E_{obs}$ ).

6

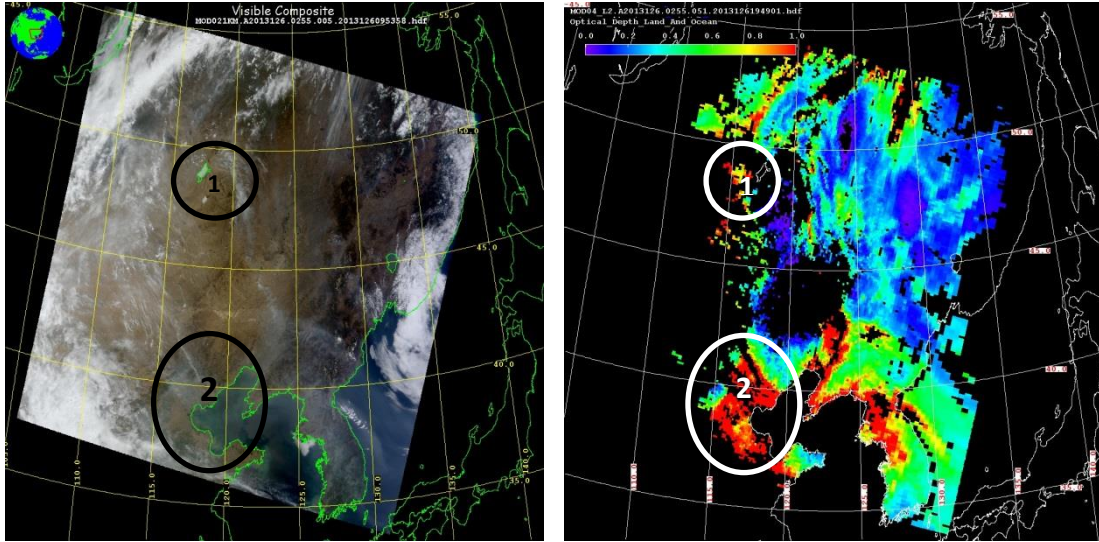


1

2

3 Figure 5. The comparison of the CHIMERE v2013 forecast (left) with OMI satellite  
 4 observations (middle) on 6 May 2013. The right plot shows the difference between  
 5 observations and forecast (OmF).

6



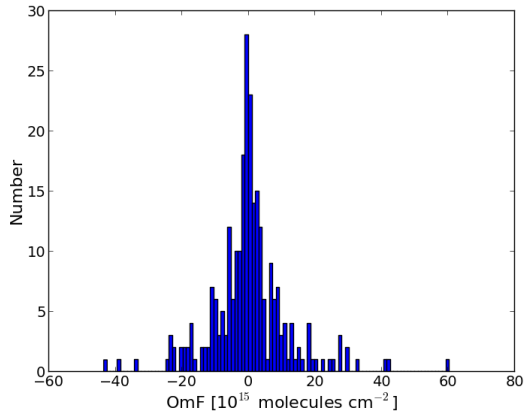
1

2

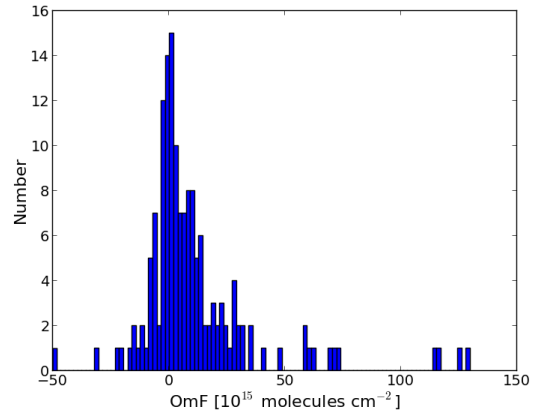
3 Figure 6. The RGB image (left) and Aerosol Optical Depth (right) from MODIS on 6 May  
 4 2013. Circle 1 and circle 2 represent the Hulunbuir sand land and the Bohai Bay respectively.  
 5 (The figures are from [https://ladsweb.nascom.nasa.gov/browse\\_images/granule\\_browser.html](https://ladsweb.nascom.nasa.gov/browse_images/granule_browser.html))

6

7



a. April to September 2013



b. October 2013 to March 2014

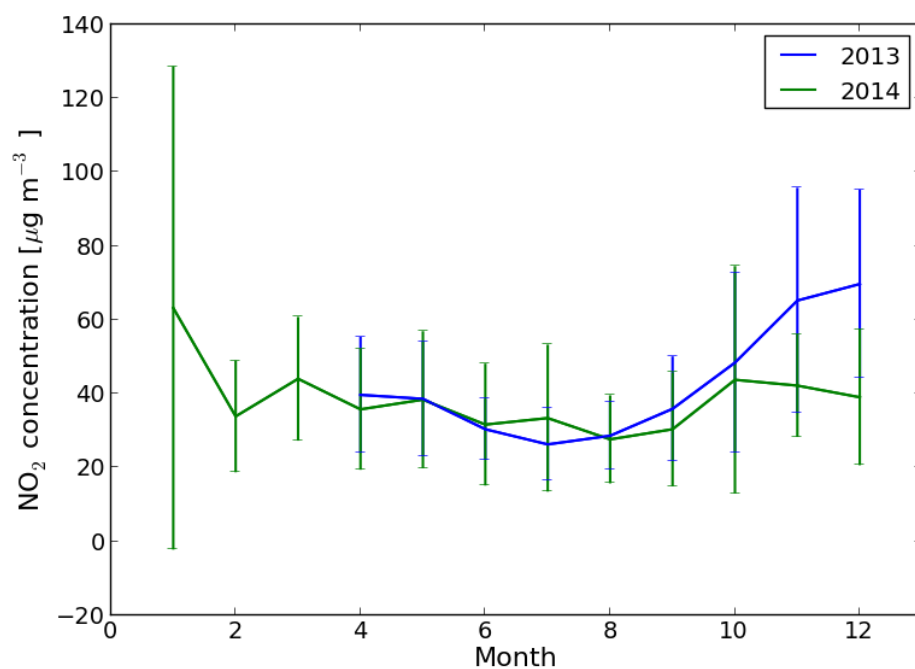
1

2

3 Figure 7. The distribution of the OmF values over 15 polluted cities in summer (a) and in  
 4 winter (b). The 15 polluted cities are Baoding, Beijing, Chengdu, Harbin, Hohhot,  
 5 Guangzhou, Jinan, Shanghai, Shenyang, Shijiazhuang, Tianjin, Wuhan, Xi'an, Xingtai and  
 6 Zhengzhou.

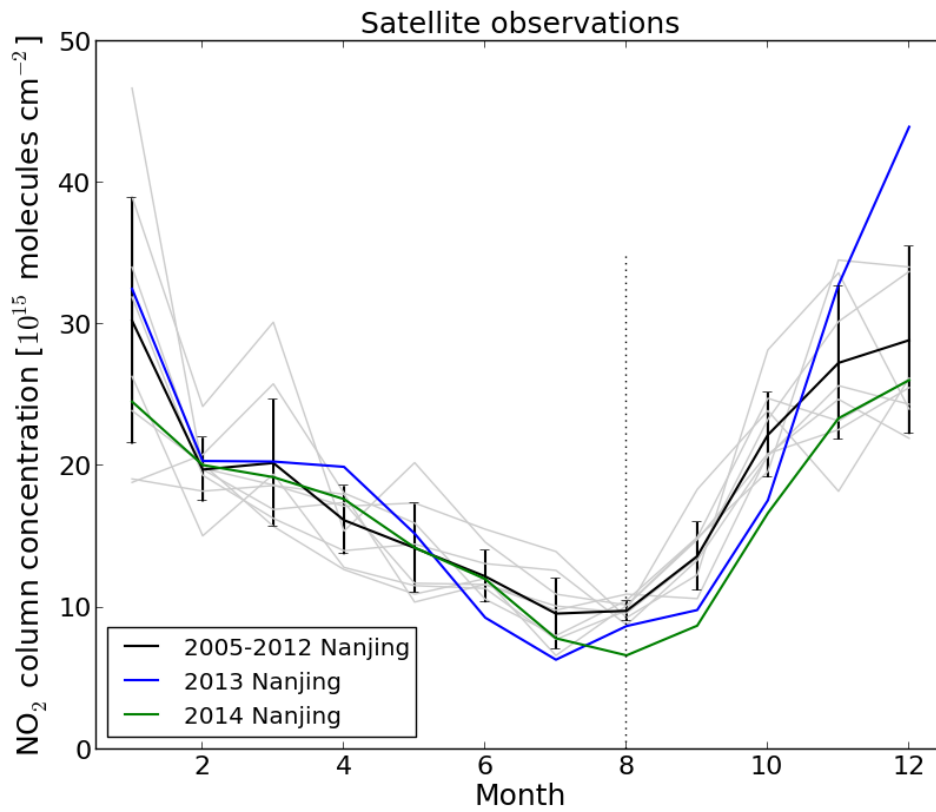
7

8



1  
2  
3  
4  
5  
6

Figure 8. The monthly averaged in-situ NO<sub>2</sub> concentration at 13 local time in Nanjing for 2013 and 2014. The bar is the standard deviation (natural variability) of the observations for each month (derived from the daily data on [www.aqicn.org](http://www.aqicn.org)).



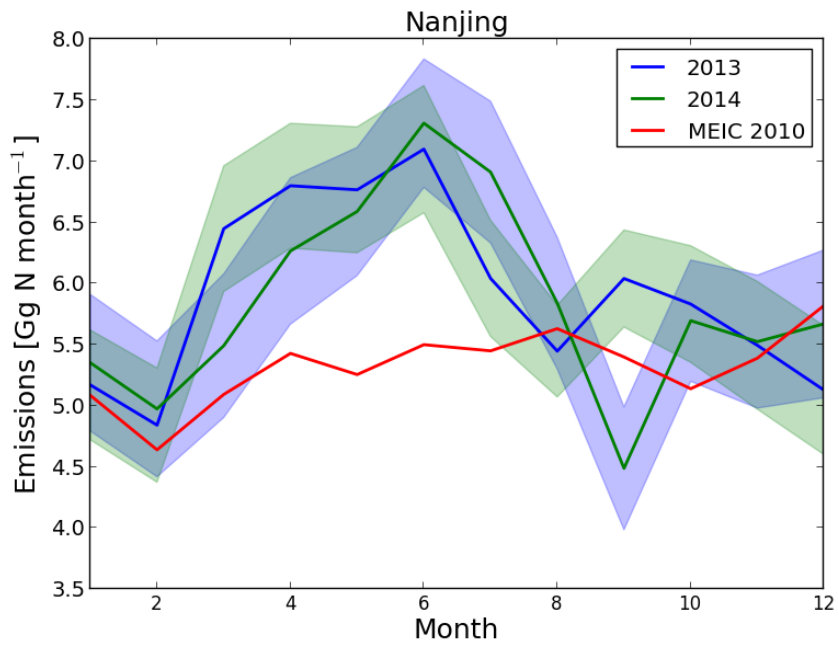
1

2

3 Figure 9. The monthly averages of OMI satellite observations of tropospheric NO<sub>2</sub>  
 4 concentrations. The solid lines are the measurements over the Nanjing area. The grey lines  
 5 are the monthly averages for each year from 2005 to 2012 to indicate the annual variability.  
 6 The black lines show the average value for the years from 2005 to 2012. The bars are the  
 7 standard deviations of monthly NO<sub>2</sub> observations from 2005 to 2012.

8

9



1

2

3 Figure 10. The monthly NO<sub>x</sub> emission estimates by DECSO in Nanjing for 2013 (blue line)  
 4 and 2014 (green line) and the monthly NO<sub>x</sub> emission of the MEIC inventory of 2010 (red  
 5 line). The shade areas show the error of the mean NO<sub>x</sub> emission estimates from DECSO.

6